Full Paper

Journal of the Brazilian Chemical Society

https://dx.doi.org/10.21577/0103-5053.20260066

J. Braz. Chem. Soc. **2026**, *37*, e-20260066, 1-13

Synthesis of Caffeine Derivatives and Evaluation of Their Anticholinesterase Activities

Gabriela M. Furlani,[a] *Júnio G. Silva,*[b] *Luana L. Dutra,*[c] *João P. V. Leite,*[c] *Felipe T. Martins,*[d] *Antonio J. Demuner,*[*,a] *Eduardo V. V. Varejão*[a] *and Marcelo H. dos Santos*[a]

[a]*Departamento de Química, Universidade Federal de Viçosa, Campus Universitário, 36570-900 Viçosa-MG, Brazil*

[b]*Departamento de Química, Universidade Federal de Minas Gerais, Pampulha, 31270-901 Belo Horizonte-MG, Brazil*

[c]*Departamento de Bioquímica e Biologia Molecular, Universidade Federal de Viçosa, Campus Universitário, 36570-900 Viçosa-MG, Brazil*

[d]*Instituto de Química, Universidade Federal de Alfenas, Centro, 37130-001 Alfenas-MG, Brazil*

Owing to the broad medicinal and agrochemical applications of cholinesterase inhibitors, the search for new molecules exhibiting this activity, particularly those with novel structural frameworks, is of great interest. Caffeine was selected as the base scaffold for the synthesis of new anticholinesterase compounds due to its neuroprotective effects and its favorable blood-brain barrier permeability constant, which facilitates action in the central nervous system. In this study, six caffeine derivatives were synthesized (yields ranging from 51-95%), incorporating functional groups inspired by commercially available acetylcholinesterase (AChE) inhibitors. Among the compounds obtained, the brominated analog (CAF-Br (**2**)) stood out by exhibiting the highest inhibitory activity against AChE (55% inhibition at 50 μmol L^{-1}). Computational studies conducted herein suggest that the formation mechanism of this derivative most likely proceeds via an electrophilic aromatic substitution (S_EAr) pathway, rather than through a radical mechanism. In addition, molecular docking analyses, together with physicochemical parameter evaluations, indicate a possible association between smaller structural volumes and increased AChE inhibitory effects.

Keywords: semi-synthesis, caffeine, cholinesterase, ethers, molecular docking

Introduction

Cholinesterases play an essential role in both the central and peripheral nervous systems. These serine hydrolases comprise a two-member enzyme family: acetylcholinesterase (AChE) and butyrylcholinesterase (BuChE).[1-3] Under physiological conditions, AChE terminates the action of acetylcholine at synapses, serving as a critical component in the maintenance and performance of the nervous system.[1,2] In addition, AChE is implicated in embryonic stem cell differentiation, neuritogenesis, cell adhesion, synaptogenesis, activation of dopaminergic neurons, beta-amyloid fibril assembly, hematopoiesis, thrombopoiesis, and the regulation of glutamate-mediated hippocampal activity. The role of BuChE remains under considerable discussion; however, it is known to contribute significantly to cholinergic mediation, support neurogenesis, and exert a detoxifying effect on various xenobiotic drugs.[2]

Numerous compounds are isolated and synthesized with the aim of inhibiting these enzymes,[2] as anticholinesterases play a pivotal role in the treatment of various clinical conditions and also have applications in agriculture.[4,5] These substances function by inhibiting the enzymes AChE and BuChE, thereby prolonging the presence of acetylcholine (ACh) (Figure 1) in the synaptic cleft, which results in significant biological effects.[6]

Cholinesterase inhibitors exhibit a broad range of pharmacological actions that extend to the cardiovascular,[7,8] gastrointestinal,[9] and neuromuscular systems,[10] as well as applications in ophthalmology[11,12] and the management of

*e-mail: ademuner@ufv.br
Editor handled this article: Hector Henrique F. Koolen (Associate)

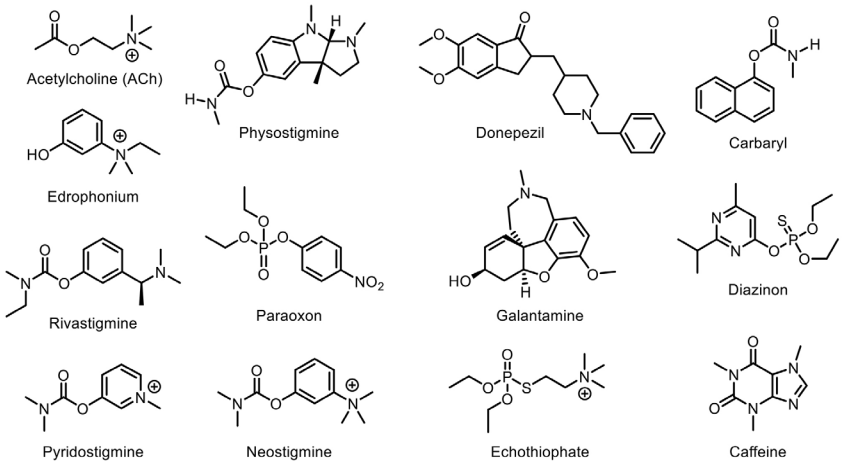

Figure 1. Chemical structures of acetylcholine (ACh), physostigmine, donepezil, galantamine, rivastigmine, neostigmine, pyridostigmine, edrophonium, paraoxon, echothiophate, diazinon, carbaryl, and caffeine.

glandular disorders.[13,14] Moreover, anticholinesterase agents are widely used as insecticides, with organophosphates and carbamates being the most common classes employed for this purpose[15] (Table 1).

Anticholinesterases can be classified according to the type of enzymatic inhibition they induce, as short-, intermediate-, or long-acting inhibitors. Short-acting inhibitors exert a competitive and reversible effect, whereas long-acting compounds form more stable intermediates with the enzyme, hindering rapid hydrolysis and thereby sustaining the anticholinesterase effect for extended periods. Depending on the type of inhibition involved, these substances may exhibit distinct biological applications[16] (Table 1).

Although the use of cholinesterase inhibitors provides beneficial therapeutic effects, their clinical application is still constrained by limited side effects. In this context, the development of novel inhibitors with enhanced selectivity toward either AChE or BuChE, while offering more favorable safety profiles, is of fundamental importance.[26]

In the agrochemical sector, prolonged use of pesticides has contributed to the development of resistance in various insect species.[27] The development of more selective

Table 1. Application of anticholinesterases and description of their mode of action

Application	Description	Examples of pharmaceuticals and agrochemicals
Central nervous system (CNS)	some lipophilic anticholinesterase agents are capable of crossing the blood-brain barrier and are effective in treating the symptoms of neurodegenerative diseases such as Alzheimer's disease,[17-21] Parkinson's disease[17,22] and dementia with Lewy bodies[23]	physostigmine, donepezil, galantamine, rivastigmine
Neuromuscular system	anticholinesterase agents prolong the presence of acetylcholine at the synapse, making them useful for reversing postoperative neuromuscular blockade and for the treatment of myasthenia gravis[10]	neostigmine, pyridostigmine, edrophonium
Cardiovascular system	cholinesterase inhibitors prolong vagal nerve action on the heart, thereby reducing heart rate (bradycardia), and are useful in the management of certain arrhythmias[7,8,20]	donepezil, rivastigmine
Gastrointestinal system	cholinesterase inhibitors enhance gastrointestinal motility and secretions[9]	paraoxon
Ophthalmology	compounds with anticholinesterase activity are used to reduce intraocular pressure by facilitating the outflow of aqueous humor and are particularly useful in the treatment of glaucoma[11,12]	echothiophate, rivastigmine, edrophonium
Secretory glands	cholinesterase inhibitors enhance the activity of cholinergic glands, such as salivary, sweat, and lacrimal glands, making them useful in cases of hyposecretion; however, their use is limited by adverse effects at higher doses[13,14]	physostigmine
Agrochemical (insecticides)	anticholinesterase agents can irreversibly inhibit insect pest AChE or BuChE, leading to severe neuronal and cognitive dysfunction, respiratory distress, loss of endurance, and death[24,25]	diazinon, carbaryl

AChE: acetylcholinesterase; BuChE: butyrylcholinesterase.

and specific inhibitors, particularly those derived from renewable and sustainable sources such as caffeine, may reduce the harmful effects on the ecosystem caused by conventional insecticides.[28,29]

In this context, the present work aims to obtain new anticholinesterase agents. To this end, we employed caffeine as the base structure, functionalizing it with moieties promising for the inhibitory action against AChE and BuChE enzymes. Caffeine (1,3,7-trimethyl-3,7-dihydro-1*H*-purine-2,6-dione) (**1**) (Figure 1), a natural methylxanthine, exhibits a multifaceted effect on the human brain, primarily through its role as an adenosine antagonist.[30] By binding to adenosine A1 and A2A receptors on neurons, caffeine blocks the inhibitory effect of adenosine on neural activity, thereby promoting increased vigilance and alertness.[31]

Due to its stimulant and neuroprotective properties,[32,33] caffeine emerges as a relevant chemical scaffold for the development of new cholinesterase inhibitors. Caffeine derivatives have demonstrated efficacy as adenosine antagonist,[34] antioxidants,[35,36] antiproliferative agents,[37] and neuroprotective compounds.[38] Furthermore, owing to its lipophilic nature and relatively small molecular size, caffeine efficiently crosses the blood-brain barrier, with a permeability coefficient of 93.3×10^{-6} cm s^{-1},[39] which is advantageous for drug development targeting the central nervous system.[19]

According to Pohanka and Dobes,[40] caffeine demonstrated the ability to inhibit acetylcholinesterase (AChE), with an inhibition constant (K_i) of 175 μmol L^{-1}. Another study by Fabiani *et al.*[41] reported a half-maximal inhibitory concentration (IC_{50}) value of 87 μmol L^{-1} for caffeine in the inhibition of acetylcholinesterase. Additionally, in the same study, theobromine derivatives also inhibited AChE, with compound **11** showing an IC_{50} value of 0.22 μmol L^{-1}. In the most recent study by Sharma *et al.*[42] an IC_{50} of 128 μmol L^{-1} was determined for caffeine, confirming its moderate anticholinesterase activity. In the same study, the introduction of an amide group into the caffeine structure resulted in a significant increase in inhibitory activity, with derivative **6i** exhibiting a reduced IC_{50} of 1.32 μmol L^{-1}.

Beyond the aforementioned biological activities of caffeine, which may act synergistically with the potential anticholinesterase effect of the derivatives targeted in this work, caffeine aligns with sustainability demands in both the pharmaceutical and agrochemical sectors because it can be sustainably sourced from plants.[43,44] Moreover, it represents a promising structural scaffold due to its innovative framework. This aspect is particularly relevant in the agrochemical field, considering the development of insect resistance to commercial products that are structurally distinct from caffeine.

Results and Discussion

Synthesis

Caffeine (**1**), one of the most notable and well-known constituents of coffee, was chemically modified to produce a series of six derivatives (Scheme 1), with CAF-Br (**2**), CAF-Ethanolamine (**3**), CAF-Phenol (**4**), CAF-*p*-Cresol (**5**), CAF-Tyrosol (**6**), and CAF-Paracetamol (**7**) being novel compounds. The moieties added to the caffeine structural scaffold were selected based on molecules known to exhibit anticholinesterase activity (Scheme 1).

One of the groups employed mimics the structure of acetylcholine, the natural substrate of AChE, while the others are present in inhibitors previously reported in the

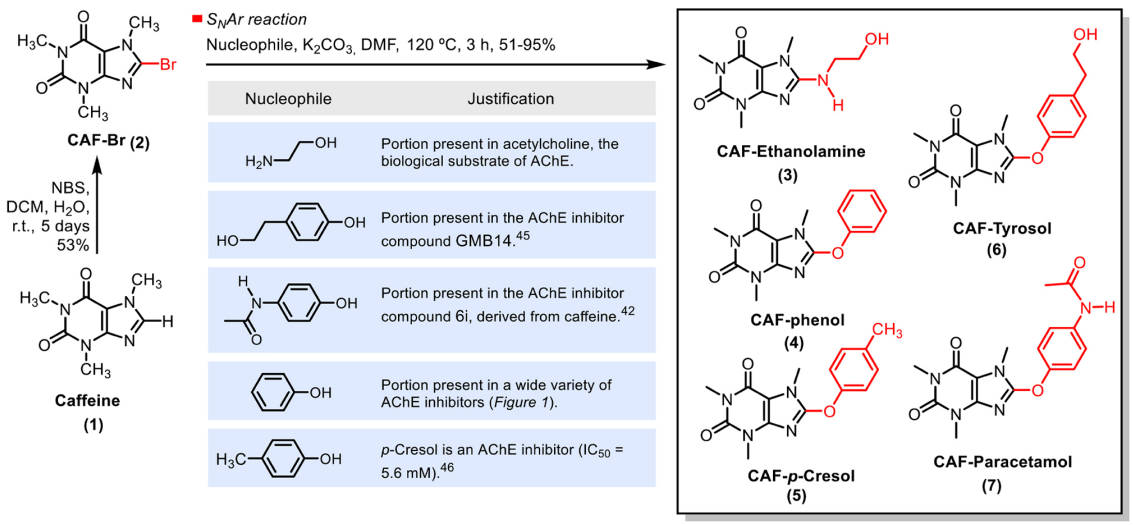

Scheme 1. Synthetic route employed for the preparation of caffeine derivatives and rationale for the choice of substituent groups in the natural product.

literature,[42,45,46] such as compounds GMB14[45] and **6i**,[42] or frequently occur in different classes of inhibitors, as is the case with benzene derivatives. This approach aimed to incorporate structural units with the potential for favorable interactions with the enzyme, allowing for the evaluation of how different substitution patterns influence the biological activity of the new molecules.

The chemical transformations on the natural product scaffold began with bromination of the imidazole core. For this purpose, NBS (*N*-bromosuccinimide) was employed. This reagent is commonly associated with radical mechanisms in bromination reactions.[47-50] However, bromination of caffeine with NBS did not yield the expected product via this pathway (Schemes 2a and 2b). The energy calculations performed in this study indicate that the intermediate leading to the formation of product CAF-Br (**2**) (**I.1**) has significantly higher energy than that associated with the radical generated at the methylene carbon bonded to the nitrogen of the imidazole ring (**I.4**). This radical is stabilized by resonance with the imidazole π system, contributing to its greater energetic favorability. It should be noted that the computational analysis presented herein considers only stationary species and relative energies, and does not include the investigation of kinetic parameters or transition states, which may play a determining role in fast reactions.

This result suggests that the reaction proceeded predominantly via an electrophilic aromatic

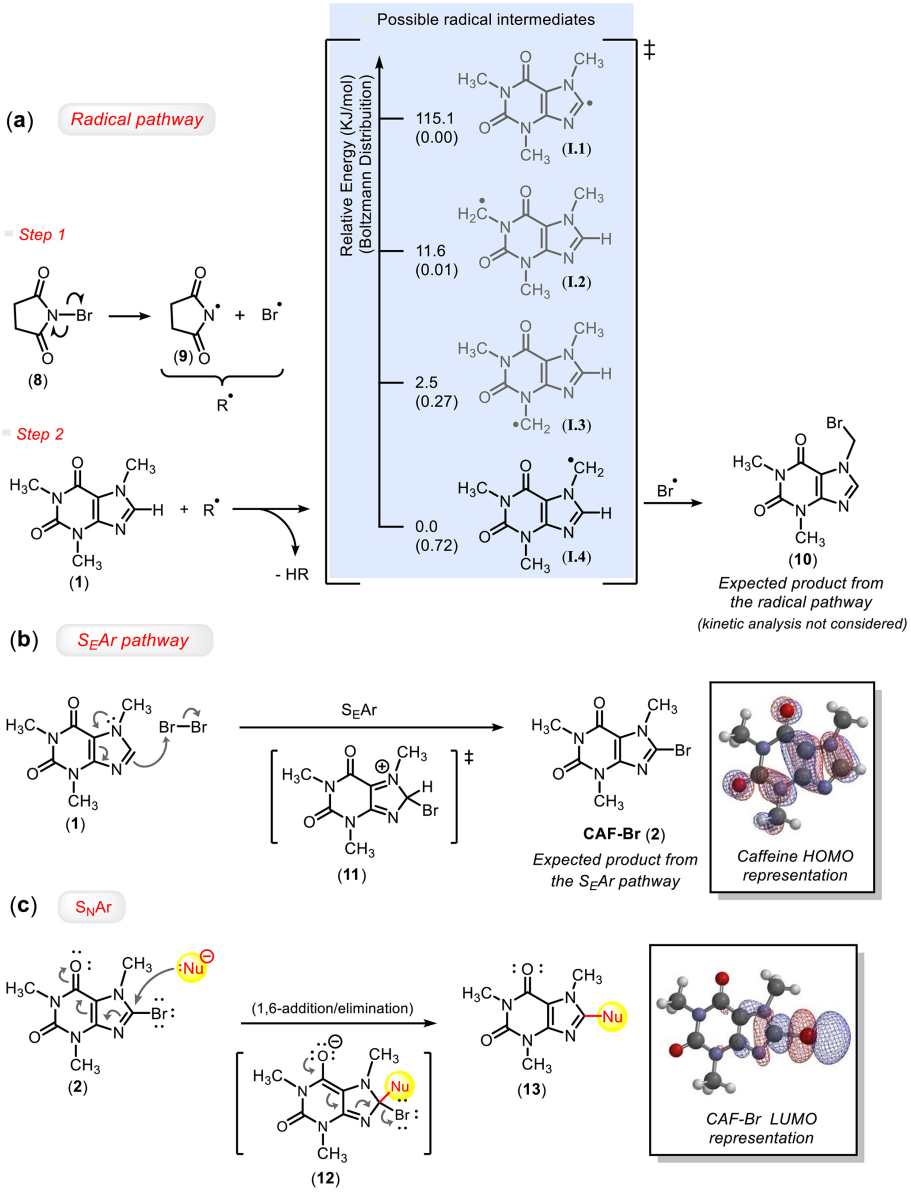

Scheme 2. (a) Relative comparison between the energy values of possible radicals formed in the caffeine structure, (b) proposed mechanisms for the bromination reaction of caffeine (**1**) via S_EAr, and (c) S_NAr. Energy values calculated using DFT – B3LYP/6-311+G(d,p).

substitution (S_EAr) mechanism, in which NBS acts as a slow source of Br_2 generated *in situ*, promoting the bromination of caffeine. Maske *et al.*[51] describe a mechanism similar to that proposed in Scheme 2b for the bromination of caffeine via an electrophilic aromatic substitution (S_EAr) pathway. The only difference is that they use a Br_2 solution instead of NBS.

Furthermore, to test our hypothesis, we performed the bromination of caffeine using Br_2, under light-protected conditions and in the presence of the radical inhibitor 2,2,6,6-tetramethylpiperidine-1-oxyl (TEMPO). CAF-Br (**2**) was the only product detected, which supports the hypothesis that, in the reaction employing NBS, Br_2 is slowly generated in the reaction medium and bromination occurs predominantly via a S_EAr pathway rather than a radical mechanism.

The synthesis of the other caffeine derivatives was carried out from CAF-Br (**2**) via nucleophilic aromatic substitution (S_NAr) reactions (Scheme 2c)[52,53] employing phenoxides or an amine as nucleophiles. Through comparative nuclear magnetic resonance (NMR) analyses of caffeine and the spectra obtained from the reaction products, as well as interpretation of infrared spectra and high-resolution mass spectrometry analyses, the success of the reactions was confirmed. For the derivatives containing the benzene ring, characteristic signals of this unit were observed in the ^{1}H NMR spectrum between δ 6.5-7.5, and in the ^{13}C NMR spectrum between δ 115-140, confirming the presence of aromatic systems. In the case of the CAF-Ethanolamine (**3**) derivative, signals attributed to the aliphatic portion appeared between δ 2.5-4.0 in the ^{1}H NMR spectrum, and between δ 40-60 in the ^{13}C NMR spectrum. In the infrared spectroscopy region, typical stretching bands of the hydroxyl group (O–H) were detected between 3200 and 3500 cm^{-1}, characteristic of compounds containing this functionality (CAF-Ethanolamine (**3**) and CAF-Tyrosol (**6**)). Additionally, the compounds CAF-Tyrosol (**6**) and CAF-Ethanolamine (**3**) produced suitably sized crystals for structural determination by X-ray diffraction (Figures 2-4 and Supplementary Information (SI) section).

CAF-Tyrosol (**6**) and CAF-Ethanolamine (**3**) were crystallized with one molecule in the asymmetric unit belonging to the monoclinic space groups $P2_1$ and $P2_1/c$, respectively (Figure 2). If not considered the terminal CH_2OH tail, the molecular backbone of CAF-Tyrosol (**6**) can be described by two planes crossing through the caffeine platform and the tyrosol substituent (root-mean square deviation (RMSD)) for the 14 non-hydrogen caffeine atoms fitted in the least-square plane is 0.0380 Å, while the RMSD for the chosen 8 non-hydrogen tyrosol atoms

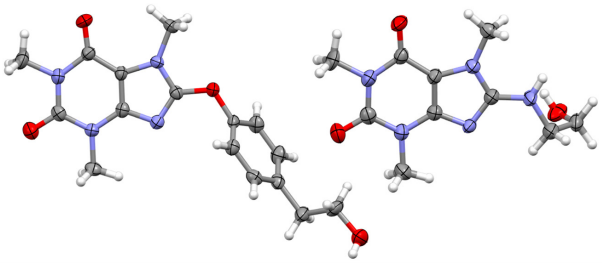

Figure 2. A 50% probability ellipsoid drawing for non-hydrogen atoms present in the asymmetric units of the CAF-Tyrosol (**6**) (left) and CAF-Ethanolamine (**3**) (right) crystal structures (hydrogens are depicted as arbitrary radius spheres).

(excluding CH_2OH) is 0.0300 Å. These planes are bent by 66.96(12)º. CAF-Ethanolamine (**3**) can be viewed as a molecular plane up to the methylene group bonded to amine (the RMSD for the 16 non-hydrogen atoms defined as the 14 caffeine ones plus its N and C neighbors is 0.0427 Å), with a CH_2OH motif appended almost perpendicularly to this plane (there is an angle of 87º between the afore defined least-square plane and that crossing the oxygen and carbons of ethanolamine substituent). This motif is also almost perpendicularly bent relative to the afore-mentioned tyrosol least-square mean plane (the corresponding angle is 81º in CAF-Tyrosol (**6**)).

Even though both compounds share the common molecular caffeine scaffold, their supramolecular architectures differ as a function of the substituent. The main supramolecular entity found in CAF-Tyrosol (**6**) is a one-dimensional chain made up of translation-symmetry related molecules held together through classical hydrogen bonds (HB) between hydroxyl and carbonyl groups (see Figure 3; D: HB donor atom, A: HB acceptor atom; D…A distance: 2.763(6) Å; D–H…A angle: 123º). This classical HB is also formed between the same groups in CAF-Ethanolamine (**3**), but giving rise to centrosymmetric dimer in this crystal structure (Figure 4, D…A distance: 2.815(7) Å; D–H…A angle: 165º). These dimers are further cross-linked through another classical HB involving the NH moiety as donor and the OH oxygen as acceptor (Figure 4, D…A distance: 2.865(7) Å; D–H…A angle: 151º).

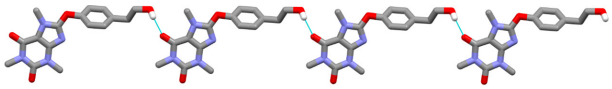

Figure 3. The one-dimensional chain formed in the crystal packing of CAF-Tyrosol (**6**) by means of OH…O hydrogen bonds (cyan lines). CH hydrogens were omitted for the sake of clarity.

Biological evaluation

Caffeine and its derivatives were evaluated for anticholinesterase activity against the AChE enzyme

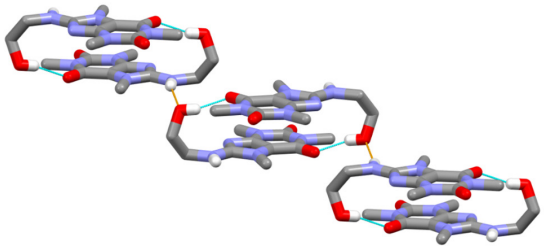

Figure 4. Crystal architecture of CAF-Ethanolamine (**3**) is mainly featured by dimers bonded by OH…O interactions (cyan lines), which are secondarily contacted by NH…O hydrogen bonds (orange lines). CH hydrogens were omitted for the sake of clarity.

from *Electrophorus electricus*. A structural comparison between this enzyme and human AChE revealed a root mean square deviation (RMSD) value of 0.63 Å-within the range considered indicative of significant homology (RMSD ≤ 2 Å).[54-56] Nevertheless, despite the high structural similarity, differences in amino acid composition and local flexibility between *E. electricus* and human AChE may influence ligand-enzyme interactions, and thus caution is required when extrapolating these results to the human enzyme.

The inhibitory effect of caffeine on AChE has been reported in two different studies[40,42] showing 50% inhibition of enzymatic activity at concentrations of 175 and 128 μmol L^{-1}. In the present study, caffeine was evaluated at a concentration of 50 μmol L^{-1} and exhibited no inhibitory activity against AChE (Table 2).

Table 2. Percentage of AChE inhibition by caffeine and its derivatives (means ± standard deviation)

Compound (50 μmol L^{-1})	Inhibition / %
Caffeine (**1**)	00.0 ± 0.0[a]
CAF-Br (**2**)	55.3 ± 5.8[b]
CAF-Ethanolamine (**3**)	00.0 ± 0.0[a]
CAF-Phenol (**4**)	13.2 ± 2.8[c]
CAF-p-Cresol (**5**)	5.7 ± 1.9[d]
CAF-Tyrosol (**6**)	5.2 ± 2.1[d]
CAF-Paracetamol (**7**)	11.4 ± 2.0[c]
Galantamine	96.0 ± 2.1[e]

Galantamine: positive control. Letters indicate significant differences at $p < 0.05$. Different letters denote statistically significant differences between values.

Among the compounds evaluated, given that the analysis was performed at only a single concentration and therefore has a qualitative character, only the CAF-Br (**2**) derivative exhibited significant anti-AChE activity, with an inhibition rate of 55.3% at a concentration of 50 μmol L^{-1}. The compounds containing a benzene ring displayed modest activity. The structural variation among CAF-Phenol (**4**), CAF-Tyrosol (**6**), and CAF-*p*-Cresol (**5**) consists, respectively, of a hydrogen, a 1-hydroxyethyl group, or a methyl group at the para position of the aromatic ring. Among these, the compound bearing a hydrogen substituent showed the highest bioactivity. The presence of an acetamide group in the same position (CAF-Paracetamol (**7**)) was also promising, exhibiting activity comparable to the hydrogen-substituted analog (CAF-Phenol (**4**)). In contrast, the presence of the 1-hydroxyethyl moiety linked to the imidazole core of caffeine via a nitrogen atom (CAF-Ethanolamine (**3**)) did not enhance the anti-AChE activity of the analog. Galantamine was used as the positive control, displaying 96.0% inhibition.

To suggest the reasons behind the observed activity of the CAF-Br (**2**) derivative, the molecular docking was conducted using the crystallized structure of AChE available in the PDB database (PDB ID: 4EY6) (Figure S25). The computational analyses were carried out using Molegro Virtual Docker® (MVD®, version 6.0.1; Molegro ApS; CLC bio, Denmark, 2013), which employs a differential evolution algorithm wherein a population of conformers undergoes random variations induced by operators such as recombination and mutation. The scoring function considers both intermolecular interactions between the protein and the ligand and the ligand's intramolecular interaction energy.[57]

The computational methodology was validated by performing a redocking of the galantamine structure originally co-crystallized with AChE (PDB 4EY6). The obtained RMSD value was 0.216 Å (reference value ≤ 2 Å).[54-56,58]

The *in silico* inhibition values presented in Table 3 correlate with those obtained in the *in vitro* assay, suggesting that the predictive methodology employed in the molecular docking analysis is well-suited. For CAF-Br (**2**), Key interactions were suggested by the docking analysis, including those with catalytic serine (Ser203) and histidine residues of the catalytic triad, as well as glycine and tryptophan residues, which play a crucial role in substrate orientation within the active site and in charge stabilization (Table 4 and Figure 5).[59-61]

Molecular docking analyses suggest that caffeine and its analogs interact within the same region as the

Table 3. Percentage of inhibition and energy values for the enzyme-substrate complexes of CAF-Br (**2**), caffeine (**1**), and galantamine, the positive control

Enzyme-ligand	*In vitro* inhibition (50 μmol L^{-1}) / %	*In silico* score / (kcal mol^{-1})
AChE - galantamine	96	−146.43
AChE - CAF-Br	55	−81.53
AChE - caffeine	0	−70.16

AChE: acetylcholinesterase; CAF: caffeine.

Table 4. Energy values for interactions between amino acid residues of AChE (4EY6) and the CAF-Br (**2**) molecule

	Amino acid or water	Energy / (kcal mol^{-1})
1	**Ala 204**	–0.35
2	Glu 202	–1.02
3	**Gly 121**	–10.10
4	**Gly 122**	–5.12
5	Gly 448	–0.85
6	**His 447**	–7.50
7	Phe 295	–2.16
8	Phe 297	–5.61
9	Phe 338	–8.95
10	Ser 125	–0.83
11	**Ser 203**	–3.63
12	**Trp 86**	–11.40
13	Trp 236	–1.05
14	Tyr 124	–8.20
15	Tyr 337	–13.05
16	H_2O 114	–1.19
17	H_2O 119	–0.53
18	H_2O 159	–3.33
19	H_2O 161	–0.43
20	H_2O 190	–1.60
21	H_2O 191	–0.39

Residues belonging to the catalytic site are highlighted in bold. Ala: alanine; Glu: glutamic acid; Gly: glycine; His: histidine; Phe: phenylalanine; Ser: serine; tryptophan; TRP: Tyr: tyrosine.

commercial inhibitor galantamine, located at the bottom of the enzymatic cavity. This region has a limited volume, such that, within the set of compounds evaluated in this study, substantial increase in molecular size resulting from structural modifications to caffeine were, in general, not favorable for the desired bioactivity. On the other hand, the insertion of a bromine atom into the imidazole ring, as suggested by docking, favored intermolecular interactions with the enzyme, particularly steric complementarity interactions with residues Phe338, Phe295, His447, Phe297, and Gly122, which contributed to the significant inhibitory activity observed for the CAF-Br derivative. It should be noted, however, that this observation is based on a limited dataset comprising six compounds and therefore represents a preliminary trend rather than a definitive structure-activity relationship.

Although only the CAF-Br (**2**) derivative exhibited notable AChE inhibitory activity, all caffeine analogs produced in this study were designed to comply with Lipinski's Rule of Five for drug development,[62] as well as the agrochemical-likeness criteria proposed by Hao *et al.*[63] The physicochemical parameters: MLogP (LogP calculated by the Moriguchi methodology), MW (molecular weight), HBA (acceptors of hydrogen bond), HBD (donors of hydrogen bond), CLogP (LogP calculated), ROB (rotational bonds), and ARB (aromatic bonds) for the caffeine derivatives are presented in Table 5.

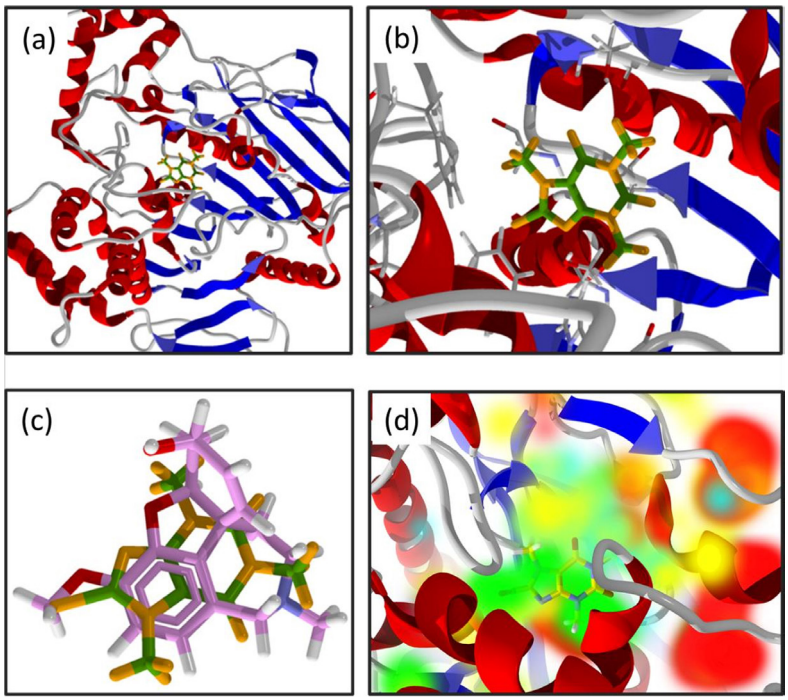

Figure 5. (a) Molecular docking of the compound CAF-Br (**2**) in AchE; (b) enlarged view of the representation in (a); (c) overlay of the lowest-energy pose of CAF-Br (**2**) (green and yellow) and galantamine (pink) crystallized in AchE; (d) representation of the lowest-energy pose of CAF-Br (**2**) in AChE. Color highlights indicate regions of steric interactions: green; hydrogen bond acceptor regions: blue; hydrogen bond donor regions: yellow; and electrostatic interaction regions: red.

Table 5. *In silico* parameters with data from Lipinski[62] and Hao *et al.*[63] for the compounds

Compound	MLogP	MW / (gmol^{-1})	HBA	HBD	CLogP	ROB	ARB
Caffeine (**1**)	–0.19	194.19	3	0	–0.0403	0	9
CAF-Br (**2**)	0.55	273.09	3	0	0.857	0	9
CAF-Ethanolamine (**3**)	–0.48	253.26	4	2	–0.251	3	9
CAF-Phenol (**4**)	1.46	286.29	4	0	2.057	2	15
CAF-*p*-Cresol (**5**)	1.71	300.31	4	0	2.556	2	15
CAF-Tyrosol (**6**)	1.17	330.34	5	1	1.248	4	15
CAF-Paracetamol (**7**)	1.00	343.34	5	1	1.076	4	15

References values to: MLogP (Lipinski[62] ≤ 4.15); MW (Lipinski[62] ≤ 500; Hao *et al.*[63] ≤ 435); HBA (Lipinski[62] ≤ 10; Hao *et al.*[63] ≤ 6); HBD (Lipinski[62] ≤ 5; Hao *et al.*[63] ≤ 2); CLogP (Hao *et al.*[63] ≤ 6); ROB (Hao *et al.*[63] ≤ 9); ARB (Hao *et al.*[63] ≤ 17). MLogP: LogP calculated by the Moriguchi methodology, MW: molecular weight, HBA: acceptors of hydrogen bond; HBD: donors of hydrogen bond; CLogP: LogP calculated; ROB: rotational bonds; ARB: aromatic bonds.

The molecular properties of compounds were calculated by the platform Swiss Institute of Bioinformatics (SwissADME®, swiss-model, version 4.1.0).[64] The CLogP was calculated in Spartan'14 (Spartan'14, version 1.1.4; Wavefunction, Inc., Irvine, 2014).[65]

Conclusions

Six caffeine derivatives were synthesized (yields ranging from 51-95%), each incorporating chemical moieties commonly found in some commercial AChE inhibitors. Among these compounds, the CAF-Br derivative exhibited the highest percentage of enzyme inhibition (55% inhibition at 50 μmol L^{-1}). The reaction mechanism for the formation of this derivative was investigated computationally, suggesting that the reaction proceeds via an electrophilic aromatic substitution pathway, rather than through a radical mechanism. Molecular docking studies suggest that the small molecular size of CAF-Br (**2**), along with the steric distortion in AChE induced by the bromine atom, are key factors contributing to the observed activity. Although the inhibition percentage is lower than that of the positive control (galantamine, 96%), this structure appears promising, as it represents a novel structural scaffold with anti-AChE activity. This characteristic is relevant both in the context of acquired resistance to agrochemicals acting via this mechanism and in the development of new anti-AChE drug candidates.

Experimental

General information

All solvents and reagents used were of analytical grade. Column chromatography was performed using silica gel (230-400 mesh). Reaction monitoring was conducted via thin-layer chromatography (TLC) on pre-coated silica gel plates with aluminum backing (Macherey-Nagel DC-Fertigfolien ALUGRAM® Xtra SIL G/UV254). TLC plates were visualized under UV light (λ = 254 nm). Infrared (IR) spectra were recorded using a VARIAN 660-IR spectrophotometer (Varian, Palo Alto, CA, USA) equipped with a GladiATR accessory, scanning in the range of 4000 to 500 cm^{-1} and absorption bands are reported in cm^{-1}. ^{1}H nuclear magnetic resonance (NMR) (400 MHz) and ^{13}C NMR (100 MHz) spectra were obtained on a Bruker 400 MHz spectrometer (Billerica, Massachusetts, USA) at 25 °C. Chemical shifts (δ) are expressed in ppm relative to tetramethylsilane (TMS) (Me_4Si) or deuterated solvent ($CDCl_3$, CD_3OD) and the coupling constants (J) are expressed in Hz. Melting points were measured using an MQAPF-302 Microchemistry apparatus (Microquímica Equipamentos, Palhoça, Santa Catarina, Brazil). High-resolution mass spectrometry (HRMS) of final products was performed on a Bruker Impact II UHRQqTOF MS (Bruker Daltonics, Bremen, Germany), equipped with an electrospray ionization source operating in positive ion mode and ions were detected as protonated or adducted species ($[M + H]^+$). Data acquisition was conducted using the Otof Control and Hystar software packages (Bruker Daltonics, Bremen, Germany). Single-crystal X-ray diffraction data for compounds CAF-Tyrosol (**6**) and CAF-Ethanolamine (**3**) were collected using a Bruker diffractometer (Bruker Daltonics, Billerica, USA) equipped with an APEX II CCD detector at room temperature (23 °C). Graphite-monochromated MoKα radiation with a wavelength (λ) of 0.71073 A was employed.

Synthesis

Synthesis of the derivative 8-bromo-1,3,7-trimethyl-3,7-dihydro-1*H*-purine-2,6-dione (CAF-Br) (**2**)

The compound CAF-Br (**2**) was synthesized following the methodology described by Arsenyan *et al.*[66] To a round-bottom flask, caffeine (10 mmol; 1 eq), NBS

(20 mmol; 2 eq), and CH_2Cl_2 (30 mL) were added. The reaction mixture was stirred until the solids were completely dissolved. Subsequently, distilled water (10 mL) was added, and the reaction was stirred for five days. After this period, an aqueous solution of NaOH (2.5 M, 10 mL) was added, and stirring continued until decolorization occurred. The organic phase was then separated, washed with water (3 × 40 mL), dried over anhydrous Na_2SO_4, and evaporated under reduced pressure. The desired product was obtained as a white solid; yield 53%; Rf (ethyl acetate) 0.69; mp 208.9-209.6 °C; IR attenuated total reflectance (ATR) / cm^{-1} 1701, 1652, 1448, 1340, 741; ^{1}H NMR (400 MHz, $CDCl_3$) δ 3.94 (s, 3H), 3.53 (s, 3H), 3.37 (s, 3H); ^{13}C NMR (100 MHz, $CDCl_3$) δ 155.5, 151.8, 148.7, 141.5, 107.6, 33.7, 29.8, 28.0; HRMS (ESI) *m/z*, calcd. for $C_8H_9BrN_4O_2$ $[M + H]^+$: 272.9909, found: 272.9983. The spectroscopic data were consistent with those reported in the literature.[67]

Synthesis of the derivative 8-((2-hydroxyethyl)amino)-1,3,7-trimethyl-3,7-dihydro-1*H*-purine-2,6-dione (CAF-Ethanolamine) (**3**)

The compound CAF-Ethanolamine (**3**) was synthesized according to the adapted methodology described by Georgieva *et al.*[68] To a reaction tube, CAF-Br (**2**) (0.366 mmol) and ethanolamine (230 µL) were added. The reaction mixture was stirred for 2 h at 130 °C. The compound was purified by silica gel column chromatography, using an ethanol-ethyl acetate mixture (1:2 v/v) as the eluent. Finally, the product was concentrated under reduced pressure. The desired product was obtained as a colorless crystal; Rf (ethyl acetate / ethanol 2:1) 0.38; mp 208.6-210.4 °C; yield 95%; IR (ATR) / cm^{-1} 3349, 3239, 2961, 1690, 1624, 1351, 1220, 745; ^{1}H NMR (400 MHz, CD_3OD) δ 4.86 (s,1H), 4.02 (t, *J* 5.7 Hz, 2H), (s, 3H), 3.84 (t, *J* 5.7 Hz, 2H), 3.49 (s, 3H), 3.32 (s, 3H); ^{13}C NMR (100 MHz, CD_3OD) δ 155.3, 154.3, 152.3, 150,7, 103.1, 60.8, 39.5, 29.8, 27.7, 22.6; HRMS (ESI) *m/z*, calcd. for $C_{10}H_{15}N_5O_3$ $[M + H]^+$: 254.1208 found: 254.1245.

Synthesis of the derivatives from phenolic compounds (**4-7**)

The compounds were synthesized according to the adapted methodology described by Kadi *et al.*[69] To a reaction tube, CAF-Br (**2**) (0.366 mmol; 1 eq), the corresponding phenol (0.366 mmol; 1 eq), dry K_2CO_3 (0.366 mmol; 1 eq), and anhydrous dimethylformamide (DMF, 1 mL) were added. The reaction system was maintained at 120 °C for 3 h under a nitrogen atmosphere. After the reaction mixture reached room temperature, water (5 mL) was added, followed by liquid-liquid extraction with ethyl acetate (4 × 10 mL). The organic phase was dried over anhydrous Na_2SO_4 and concentrated under reduced pressure. Subsequently, all compounds were purified by silica gel column chromatography. A hexane/EtOAc mixture in a 1:1 (v/v) ratio was used as the eluent for CAF-Phenol (**4**) and CAF-Tyrosol (**6**), a 2:1 (v/v) ratio for CAF-*p*-Cresol (**5**), and ethyl acetate alone for CAF-Paracetamol (**7**).

1,3,7-Trimethyl-8-phenoxy-3,7-dihydro-1*H*-purine-2,6-dione (CAF-Phenol) (**4**)

The desired product was obtained as a white solid; Rf (hexane/ethyl acetate 2:1) 0.32; mp 140-142 °C; yield 95%; IR (ATR) / cm^{-1} 1700, 1646, 1592, 1515, 1443, 1282, 1202, 742; ^{1}H NMR (400 MHz, $CDCl_3$) δ 7.47-7.40 (m, 2H), 7.34-7.24 (m, 3H), 3.89 (s, 3H), 3.47 (s, 3H), 3.42 (s, 3H); ^{13}C NMR (100 MHz, $CDCl_3$) δ 154.9, 153.4, 151.7, 145.9, 129.8, 125.7, 119.4, 103.8, 30.4, 29.9, 27.8; HRMS (ESI) *m/z*, calcd. for $C_{14}H_{14}N_4O_3$ $[M + H]^+$: 287.1179, found: 287.1172.

1,3,7-Trimethyl-8-(*p*-tolyloxy)-3,7-dihydro-1*H*-purine-2,6-dione (CAF-*p*-Cresol) (**5**)

The desired product was obtained as a light beige solid; Rf (hexane/ethyl acetate 2:1) 0.26; mp 101.6-103.4 °C; yield 76%; IR (ATR) / cm^{-1} 2951, 2924, 1709, 1653, 1498, 1447, 1200, 741; ^{1}H NMR (400 MHz, $CDCl_3$) δ 7.24-7.11 (m, 4H), 3.85 (s, 3H), 3.43 (s, 3H), 3.39 (s, 3H), 2.36 (s, 3H); ^{13}C NMR (100 MHz, $CDCl_3$) δ 155.0, 153.9, 151.8, 151.3, 146.0, 135.5, 130.3, 119.4, 103.8, 30.5, 30.0, 28.0, 21.0; HRMS (ESI) *m/z*, calcd. for $C_{15}H_{16}N_4O_3$ $[M + H]^+$: 301.1256, found: 301.1275.

8-(4-(2-Hydroxyethyl)phenoxy)-1,3,7-trimethyl-3,7-dihydro-1*H*-purine-2,6-dione (CAF-Tyrosol) (**6**)

The desired product was obtained as a colorless crystal; Rf (hexane/ethyl acetate 1:3) 0.26; mp 128-130 °C; yield 90%; IR (ATR) / cm^{-1} 3383, 2945, 2876, 1698, 1645, 1498, 1445, 1202, 745; ^{1}H NMR (400 MHz, $CDCl_3$) δ 7.32-7.26 (m, 4H), 3.94-3.86 (m, 5H), 3.46 (s, 3H), 3.41 (s, 3H), 2.9 (t, *J* 6.6 Hz, 2H); ^{13}C NMR (100 MHz, $CDCl_3$) δ 155.0, 153.8, 152.0, 151.7, 146.0, 136.4, 130.4, 119.7, 63.5, 38.5, 30.5, 30.0, 28.0; HRMS (ESI) *m/z*, calcd. for $C_{16}H_{18}N_4O_4$ $[M + H]^+$: 331.1422, found: 331.1426.

N-(4-((1,3,7-Trimethyl-2,6-dioxo-2,3,6,7-tetrahydro-1*H*-purin-8-yl)oxy)phenyl)acetamide (CAF-Paracetamol) (**7**)

The desired product was obtained as a beige solid; Rf (ethyl acetate) 0.35; mp 264.4-265.9 °C; yield 51%; IR (ATR) / cm^{-1} 3324, 3135, 3047, 1685, 1639, 1519, 1473, 1235, 1017; ^{1}H NMR (400 MHz, $CDCl_3$) δ 9.19 (s, 1H),

7.52 (d, *J* 8.9 Hz, 2H), 7.13 (d, *J* 8.9 Hz, 2H), 3.76 (s, 3H), 3.33 (s, 3H), 3.24 (s, 3H), 2.07 (s, 3H); ^{13}C NMR (100 MHz, $CDCl_3$) δ 169.7, 154.9, 153.9, 151.7, 149.0, 145.9, 136.1, 121.0, 119.9, 103.8, 77.1, 30.3, 29.8, 27.8, 23.7; HRMS (ESI) *m/z*, calcd. for $C_{16}H_{17}N_5O_4$ $[M + H]^+$: 344.1344, found: 344.1352.

Crystallography

Single-crystal X-ray diffraction intensities for compounds CAF-Tyrosol (**6**) and CAF-Ethanolamine (**3**) were measured using a Bruker diffractometer (Bruker Daltonics, Billerica, USA) equipped with an APEX II CCD detector at room temperature (23 °C). Graphite-monochromated MoKα radiation with a wavelength (λ) of 0.71073 Å was employed. Data collection strategies, cell refinements, and data reductions were performed using the SHELXS program.[70] The intrinsic phasing method was used to solve all structures, which were subsequently refined using F^2 statistics. Both the solving and refinements were conducted using the SHELX software package, integrated into the WinGX[71] platform. Non-hydrogen and hydrogen atoms were refined as anisotropic and isotropic, respectively. Isotropic hydrogen displacement parameters were set to 1.2 U_{iso}(C), except for methyl and hydroxyl groups which were set to 1.5 U_{iso}(C or O). All hydrogens coordinates were refined according to the riding model with standard fixed bond lengths and angles. Molecular graphics were generated using the MERCURY (Cambridge Crystallographic Data Centre (CCDC), version 4.0)[72] software and ORTEP-3 (WinGX, version 3). Crystal data, experimental details, and refinement results are summarized in the SI section. The complete set of crystal data was deposited with the Cambridge Crystallographic Data Centre (CCDC) under deposit codes shown in Table S1, SI section. In this table, a summary of the crystal data collects, raw data treatments and the refinement statistical parameters can be found.

Enzyme inhibition assay

AChE inhibition was determined using a spectrophotometric assay in 96-well microplates (TPP, Trasadingen, Switzerland), according to the method described by Ellman *et al.*,[73] with modifications.

Caffeine and its derivatives were subjected to the AChE inhibition assay. Stock solutions were stored in a freezer and reused to prepare intermediate solutions for replicate tests. Accordingly, three microplates were used, with triplicate wells for each compound. On each assay day, the samples were solubilized using an ultrasonic bath (Sander©, Soniclean 2 model) at a frequency of 40 kHz and a temperature between 30 and 35 °C, then diluted fivefold in buffer A (50 mmol L^{-1} Tris-HCl, pH 8.0), resulting in an intermediate solution at a concentration of 500 μmol L^{-1}.

In a multichannel pipette reservoir, the following were combined: bovine serum albumin solution (5 mL, 0.1% BSA in buffer A), acetylthiocholine iodide in ultrapure water (2.4 mL, 14.5 mmol L^{-1}), and a solution of 5,5'-dithiobis-(2-nitrobenzoic acid) (DTNB) (12 mL, 3 mmol L^{-1} in buffer A containing 10 mmol L^{-1} NaCl and 20 mmol L^{-1} $MgCl_2$). Negative and positive controls were prepared using methanol and galantamine, a standard inhibitor, respectively.

To assemble the plate, 200 μL of the reaction mixture (BSA, acetylthiocholine iodide, DTNB) was added to each well, followed by 25 μL of sample or control solution in triplicate. Background absorbance was read at 405 nm and 30 °C using a microplate reader (Thermoplate, TP-reader model). For the kinetic assay, 25 μL of AChE enzyme (0.2 U mL^{-1}, 0.1% in buffer A) (*Electrophorus electricus*, Type VI, Sigma-Aldrich), diluted in BSA, was added to the wells. The plate was read (with initial shaking for 5 s, λ = 405 nm, at 30 °C) every 5 min for a total duration of 25 min. Inhibition of enzymatic hydrolysis was assessed by comparing absorbance values in the absence and presence of the enzyme. The percentage of inhibition was then calculated using equation 1:

$$\text{AChE inhibition}(\%) = \frac{\text{control absorbance} - \text{sample absorbance}}{\text{control absorbance}} \times 100 \quad (1)$$

Molecular docking

The three-dimensional (3D) structures of acetylcholinesterase from *Torpedo californica*[59] and human acetylcholinesterase complexed with galantamine[60] were obtained from the Protein Data Bank (PDB) under the accession codes 1C2O and 4EY6, respectively.

The PC Spartan® software (Spartan'14, version 1.1.4; Wavefunction, Inc., Irvine, 2014)[65] was employed to construct and optimize the 3D structures of the compounds used in this study, followed by charge calculation using the semiempirical RM1 method.[74] Using Molegro Virtual Docker® software (MVD®, version 6.0.1; Molegro ApS; CLC bio, Denmark, 2013), the binding energies of the compounds within the enzymes' active sites were calculated.

The enzyme binding sites were confined to spheres with a radius of 15 Å centered on the enzymatic cavity responsible for activity. The influence of water molecules

was considered during the docking studies, and all residues within the spheres were set as flexible. Due to the stochastic nature of the docking algorithm, 10 runs were performed for each compound, with 10 poses analyzed *per* run. Re-docking of the inhibitor crystallized within the enzyme structure was used to validate the docking protocol.

Molecular docking and re-docking procedures were performed using Molegro Virtual Docker® (MVD®, version 6.0.1; Molegro ApS; CLC bio, Denmark, 2013). The MolDock scoring function (MolDock SE algorithm), based on a piecewise linear potential (PLP), was employed to evaluate ligand-protein interactions.

To assess the degree of identity between the active site residues of human and fish acetylcholinesterase and to verify their similarity, structural alignments were performed using Swiss-PdbViewer (Swiss-PdbViewer, version 4.1.0, Nicolas Guex and Manuel C. Peitsch; Swiss Institute of Bioinformatics, Switzerland, 2010).

Physicochemical parameters for determining drug-likeness and agrochemical-likeness standards

The ADMET (absorption, distribution, metabolism, excretion, and toxicity) properties of the molecules were predicted using the online platform SwissADME (swiss-model, version 4.1.0). The molecular weigh (MW), hydrogen-bond donor (HBD), hydrogen-bond acceptor (HBA), Moriguchi-predicted octanol-water partition coefficient (MLogP), octanol-water partition coefficient (CLogP), rotational bonds (RB), and aromatic bonds (AB) are listed in Table 5.

Statistics analysis

Data are expressed as mean ± standard deviation. Statistical comparisons between groups were performed using analysis of variance (ANOVA), followed by Tukey's test to identify significant differences. Different letters above the values indicate statistically significant differences between groups ($p < 0.05$). The software used was GraphPad Prism® (GraphPad Prism, version 5.0.1; GraphPad Software, Inc., USA, 2007).[75]

In silico study of the formation mechanism of CAF-Br (**2**)

The chemical structures of the reagents, products, and possible reaction intermediates were initially constructed and subjected to geometric optimization using Density Functional Theory (DFT) with the B3LYP functional and the 6-31G** basis set. All calculations were performed using Spartan'14 software (Spartan'14, version 1.1.4; Wavefunction, Inc., USA, 2014.).[65] All calculations were carried out in vacuum (gas phase).

For radical species, calculations were performed assuming a neutral total charge and one unpaired electron (doublet spin state). Following optimization, vibrational frequency calculations were conducted to confirm the nature of the stationary points: the absence of imaginary frequencies indicated energy minima, characterizing stable structures. Subsequently, single-point energy calculations were carried out at the B3LYP/6-311+G(d,p) level on the previously optimized geometries in order to refine the electronic energy values. The total electronic energies obtained were used to compare the relative stability of the intermediates. All energies discussed correspond to relative electronic energies obtained directly from the electronic structure calculations in the gas phase and converted to kJ mol^{-1}, and were used for comparative purposes between species.

Supplementary Information

Supplementary information (spectroscopic data (IR, NMR, HRMS and X-ray diffraction), and additional data from theoretical studies) is available free of charge at http://jbcs.sbq.org.br as PDF file.

Data Availability Statement

The data supporting the findings of this study are available within the article and its SI section.

Acknowledgments

The authors gratefully acknowledge the financial support provided by FAPEMIG, CAPES, CNPq (INCT-Defesa No. 408584/2024-6; No. 409429/2025-2), Embrapa - Consórcio Café and FINEP.

Author Contributions

G. M. F.: conceptualization, methodology, investigation, resources, visualization, writing (original draft, review and editing); J. G. S.: data curation, investigation, visualization, software, validation, writing (original draft, review and editing); L. L. D. and J. P. V. L.: data curation, methodology, investigation, writing (review and editing); F. T. M.: methodology, investigation, writing (review and editing); A. J. D. and E. V. V. V.: writing (review and editing); M. H. S.: project administration, funding acquisition, supervision investigation, resources, writing (original draft, review and editing).

References

1. De Boer, D.; Nguyen, N.; Mao, J.; Moore, J.; Sorin, E. J.; *Biomolecules* **2021**, *11*, 580. [Crossref]

2. Korabecny, J.; Soukup, O.; *Biomolecules* **2021**, *11*, 1121. [Crossref]
3. Lopes, J. P. B.; da Costa, J. S.; Ceschi, M. A.; Gonçalves, C. A. S.; Konrath, E. L.; Karl, A. L. M.; Guedes, I. A.; Dardenne, L. E.; *J. Braz. Chem. Soc.* **2017**, *28*, 2218. [Crossref]
4. Colovic, M. B.; Krstic, D. Z.; Lazarevic-Pasti, T. D.; Bondzic, A. M.; Vasic, V. M.; *Curr. Neuropharmacol.* **2013**, *11*, 315. [Crossref]
5. Araújo, C. R. M.; Santos, V. L. A.; Gonsalves, A.; *Rev. Virtual Quim.* **2016**, *8*, 1818. [Crossref]
6. Silman, I.; *Prog. Biophys. Mol. Biol.* **2021**, *162*, 41. [Crossref]
7. Howes, L. G.; *Drug Saf.* **2014**, *37*, 391. [Crossref]
8. Rampa, L.; Santangelo, R.; Gaspardone, C.; Cerutti, A.; Magnani, G.; Piscazzi, F.; Sgherzi, G.; Fiore, G.; Filippi, M.; Agosta, F.; Margonato, A.; Fragasso, G.; *Am. J. Cardiol.* **2023**, *200*, 162. [Crossref]
9. Al-Mansori, A.; Al-Sbiei, A.; Bashir, G. H.; Qureshi, M. M.; Tariq, S.; Altahrawi, A.; Al-Ramadi, B. K.; Fernandez-Cabezudo, M. J.; *Heliyon* **2024**, *10*, e33849. [Crossref]
10. Katz, N. K.; Barohn, R. J.; *Neuropharmacology* **2021**, *182*, 108303. [Crossref]
11. Kim, M. J.; Ibrahim, M. M.; Jablonski, M. M.; *Front. Mol. Biosci.* **2024**, *11*, 1423351. [Crossref]
12. Wang, H.; Deng, Y.; Wan, L.; Huang, L.; *Sci. Rep.* **2020**, *10*, 9719. [Crossref]
13. Ferguson, M. M.; *Oral Surg., Oral Med., Oral Pathol.* **1993**, *75*, 186. [Crossref]
14. Khosravani, N.; Ekström, J.; Birkhed, D.; *Arch. Oral Biol.* **2007**, *52*, 1097. [Crossref]
15. Mdeni, N. L.; Adeniji, A. O.; Okoh, A. I.; Okoh, O. O.; *Molecules* **2022**, *27*, 618. [Crossref]
16. Marucci, G.; Buccioni, M.; Ben, D. D.; Lambertucci, C.; Volpini, R.; Amenta, F.; *Neuropharmacol.* **2021**, *190*, 108352. [Crossref]
17. d'Angremont, E.; Begemann, M. J. H.; Van Laar, T.; Sommer, I. E. C.; *JAMA Neurol.* **2023**, *80*, 813. [Crossref]
18. Gajendra, K.; Pratap, G. K.; Poornima, D. V.; Shantaram, M.; Ranjita, G.; *Eur. J. Med. Chem. Rep.* **2024**, *11*, 100154. [Crossref]
19. Liu, Y.; Uras, G.; Onuwaje, I.; Li, W.; Yao, H.; Xu, S.; Li, X.; Li, X.; Phillips, J.; Allen, S.; Gong, Q.; Zhang, H.; Zhu, Z.; Liu, J.; Xu, J.; *Eur. J. Med. Chem.* **2022**, *235*, 114305. [Crossref]
20. Shahim, B.; Xu, H.; Haugaa, K.; Zetterberg, H.; Jurga, J.; Religa, D.; Eriksdotter, M.; *Eur. Heart J.: Cardiovasc. Pharmacother.* **2024**, *10*, 128. [Crossref]
21. Zhang, J.; Zhang, Y.; Wang, J.; Xia, Y.; Zhang, J.; Chen, L.; *Sig. Transduction Targeted Ther.* **2024**, *9*, 211. [Crossref]
22. Bohnen, N. I.; Yarnall, A. J.; Weil, R. S.; Moro, E.; Moehle, M. S.; Borghammer, P.; Bedard, M.-A.; Albin, R. L.; *Lancet Neurol.* **2022**, *21*, 381. [Crossref]
23. Jellinger, K. A.; *J. Neural Transm.* **2018**, *125*, 615. [Crossref]
24. Aroniadou-Anderjaska, V.; Figueiredo, T. H.; de Araujo Furtado, M.; Pidoplichko, V. I.; Braga, M. F. M.; *Toxics* **2023**, *11*, 866. [Crossref]
25. Mohan, M. K.; Thorat, K.; Puthiyapurayil, T. P.; Sunnapu, O.; Chandrashekharappa, S.; Ravula, V.; Khader, R.; Sankaranarayanan, A.; Muhammad, H.; Vemula, P. K.; *Nat. Commun.* **2024**, *15*, 4844. [Crossref]
26. Sobha, A.; Ganapathy, A.; Mohan, S.; Madhusoodanan, N.; Babysulochana, A. D.; Alaganandan, K.; Somappa, S. B.; *Eur. J. Med. Chem. Rep.* **2024**, *12*, 100237. [Crossref]
27. Van Den Berg, H.; Da Silva Bezerra, H. S.; Al-Eryani, S.; Chanda, E.; Nagpal, B. N.; Knox, T. B.; Velayudhan, R.; Yadav, R. S.; *Sci. Rep.* **2021**, *11*, 23867. [Crossref]
28. Duque, J. E.; Urbina, D. L.; Vesga, L. C.; Ortiz-Rodríguez, L. A.; Vanegas, T. S.; Stashenko, E. E.; Mendez-Sanchez, S. C.; *Sci. Rep.* **2023**, *13*, 2989. [Crossref]
29. Raisch, T.; Raunser, S.; *Nat. Struct. Mol. Biol.* **2023**, *30*, 1411. [Crossref]
30. Chen, X.; Gawryluk, J. W.; Wagener, J. F.; Ghribi, O.; Geiger, J. D.; *J. Neuroinflammation* **2008**, *5*, 12. [Crossref]
31. Marcinek, K.; Luzak, B.; Rozalski, M.; *Int. J. Mol. Sci.* **2024**, *25*, 8905. [Crossref]
32. Reddy, V. S.; Shiva, S.; Manikantan, S.; Ramakrishna, S.; *Eur. J. Med. Chem. Rep.* **2024**, *10*, 100138. [Crossref]
33. Socała, K.; Szopa, A.; Serefko, A.; Poleszak, E.; Wlaź, P.; *Int. J. Mol. Sci.* **2020**, *22*, 107. [Crossref]
34. Jacobson, K. A.; Shi, D.; Gallo-Rodriguez, C.; Manning, M.; Müller, C.; Daly, J. W.; Neumeyer, J. L.; Kiriasis, L.; Pfleiderer, W.; *J. Med. Chem.* **1993**, *36*, 2639. [Crossref]
35. Jasiewicz, B.; Sierakowska, A.; Jankowski, W.; Hoffmann, M.; Piorońska, W.; Górnicka, A.; Bielawska, A.; Bielawski, K.; Mrówczyńska, L.; *Free Radical Res.* **2018**, *52*, 724. [Crossref]
36. Sierakowska, A.; Jasiewicz, B.; Piosik, Ł.; Mrówczyńska, L.; *Sci. Rep.* **2023**, *13*, 1785. [Crossref]
37. Andrs, M.; Muthna, D.; Rezacova, M.; Seifrtova, M.; Siman, P.; Korabecny, J.; Benek, O.; Dolezal, R.; Soukup, O.; Jun, D.; Kuca, K.; *RSC Adv.* **2016**, *6*, 32534. [Crossref]
38. Kasabova-Angelova, A.; Tzankova, D.; Mitkov, J.; Georgieva, M.; Tzankova, V.; Zlatkov, A.; Kondeva-Burdina, M.; *Curr. Med. Chem.* **2020**, *27*, 2021. [Crossref]
39. Hori, T.; Okae, H.; Shibata, S.; Kobayashi, N.; Kobayashi, E. H.; Oike, A.; Sekiya, A.; Arima, T.; Kaji, H.; *Nat. Commun.* **2024**, *15*, 962. [Crossref]
40. Pohanka, M.; Dobes, P.; *Int. J. Mol. Sci.* **2013**, *14*, 9873. [Crossref]
41. Fabiani, C.; Biscussi, B.; Munafó, J. P.; Murray, A. P.; Corradi, J.; Antollini, S. S.; *Mol. Pharmacol.* **2022**, *101*, 154. [Crossref]
42. Sharma, M.; Sharma, A.; Thakur, S.; Nuthakki, V. K.; Jamwal, A.; Nandi, U.; Jadhav, H. R.; Bharate, S. B.; *Bioorg. Chem.* **2023**, *139*, 106719. [Crossref]

43. Carvalho Neto, D. P. D.; Gonot-Schoupinsky, X. P.; Gonot-Schoupinsky, F. N.; *Front. Sustain.* **2021**, *2*, 697092. [Crossref]
44. Góngora, C. E.; Tapias, J.; Jaramillo, J.; Medina, R.; González, S.; Restrepo, T.; Casanova, H.; Benavides, P.; *Agronomy* **2023**, *13*, 1554. [Crossref]
45. Bousada, G. M.; de Sousa, B. L.; Furlani, G.; Agrizzi, A. P.; Ferreira, P. G.; Leite, J. P. V.; Mendes, T. A. D. O.; Varejão, E. V. V.; Pilau, E. J.; dos Santos, M. H.; *Comput. Biol. Chem.* **2020**, *88*, 107359. [Crossref]
46. Ogata, N.; Tagishi, H.; Tsuji, M.; *Chem. Pharm. Bull.* **2020**, *68*, 1193. [Crossref]
47. Sabuzi, F.; Pomarico, G.; Floris, B.; Valentini, F.; Galloni, P.; Conte, V.; *Coord. Chem. Rev.* **2019**, *385*, 100. [Crossref]
48. Walling, C.; Rieger, A. L.; Tanner, D. D.; *J. Am. Chem. Soc.* **1963**, *85*, 3129. [Crossref]
49. Yadav, N.; Sahoo, A. K.; Sarkar, D.; Moorthy, J. N.; *ChemRxiv* **2024**. [Crossref]
50. Yang, R.; Xiong, Y.; Deng, S.; Bai, J.; Song, X.-R.; Xiao, Q.; *RSC Adv.* **2023**, *13*, 33495. [Crossref]
51. Maske, P. D.; Borkar, V. T.; Latpate, S. S.; *Russ. J. Gen. Chem.* **2023**, *93*, 429. [Crossref]
52. Soltani Rad, M. N.; Behrouz, S.; Zokaei, K.; Behrouz, M.; Ghanbariasad, A.; Zarenezhad, E.; *Bioorg. Chem.* **2022**, *128*, 106062. [Crossref]
53. Soltani Rad, M. N.; Behrouz, S.; Aghajani, S.; Behrouz, M.; Zarenezhad, E.; Ghanbariasad, A.; *RSC Adv.* **2023**, *13*, 3056. [Crossref]
54. Agu, P. C.; Afiukwa, C. A.; Orji, O. U.; Ezeh, E. M.; Ofoke, I. H.; Ogbu, C. O.; Ugwuja, E. I.; Aja, P. M.; *Sci. Rep.* **2023**, *13*, 13398. [Crossref]
55. Maia, E. H. B.; Assis, L. C.; de Oliveira, T. A.; da Silva, A. M.; Taranto, A. G.; *Front. Chem.* **2020**, *8*, 343. [Crossref]
56. Pagadala, N. S.; Syed, K.; Tuszynski, J.; *Biophys. Rev.* **2017**, *9*, 91. [Crossref]
57. Guimarães, A. P.; Ramalho, T. C.; França, T. C. C.; *J. Biomol. Struct. Dyn.* **2014**, *32*, 1601. [Crossref]
58. Silva, L. B.; Ferreira, E. F. B.; Maryam; Espejo-Román, J. M.; Costa, G. V.; Cruz, J. V.; Kimani, N. M.; Costa, J. S.; Bittencourt, J. A. H. M.; Cruz, J. N.; Campos, J. M.; Santos, C. B. R.; *Molecules* **2023**, *28*, 1035. [Crossref]
59. Bourne, Y.; Grassi, J.; Bougis, P. E.; Marchot, P.; *J. Biol. Chem.* **1999**, *274*, 30370. [Crossref]
60. Cheung, J.; Rudolph, M. J.; Burshteyn, F.; Cassidy, M. S.; Gary, E. N.; Love, J.; Franklin, M. C.; Height, J. J.; *J. Med. Chem.* **2012**, *55*, 10282. [Crossref]
61. Nachon, F.; Carletti, E.; Ronco, C.; Trovaslet, M.; Nicolet, Y.; Jean, L.; Renard, P. Y.; *Biochem. J.* **2013**, *453*, 393. [Crossref]
62. Lipinski, C. A.; Lombardo, F.; Dominy, B. W.; Feeney, P. J.; *Adv. Drug Delivery Rev.* **2012**, *64*, 4. [Crossref]
63. Hao, G.; Dong, Q.; Yang, G.; *Mol. Inform.* **2011**, *30*, 614. [Crossref]
64. SwissADME®, swiss-model, version 4.1.0, Swiss Institute of Bioinformatics. [Link] accessed in September 2025
65. Hehre, W. J.; Ohlinger, W. A.; *Spartan'14* v.1.1.4.; Wavefunction, Inc., Irvine, 2014.
66. Arsenyan, P.; Vasiljeva, J.; Domracheva, I.; Kanepe-Lapsa, I.; *Chem. Heterocycl. Comp.* **2020**, *56*, 776. [Crossref]
67. Vollmann, K.; Müller, C. E.; *Heterocycle* **2002**, *57*, 871. [Link] accessed in March 2026
68. Georgieva, M.; Mitkov, J.; Momekov, G.; Zlatkov, B.; Zlatkov, A.; *World J. Pharm. Pharm. Sci.* **2014**, *3*, 60. [Link] accessed in March 2026
69. Kadi, A. A.; El-Tahir, K. E. H.; Jahng, Y.; Rahman, A. F. M. M.; *Arabian J. Chem.* **2019**, *12*, 2356. [Crossref]
70. Sheldrick, G. M.; *Acta Crystallogr., Sect. A:Found. Crystallogr.* **2008**, *64*, 112. [Crossref]
71. Farrugia, L. J.; *J. Appl. Crystallogr.* **2012**, *45*, 849. [Crossref]
72. Macrae, C. F.; Sovago, I.; Cottrell, S. J.; Galek, P. T. A.; McCabe, P.; Pidcock, E.; Platings, M.; Shields, G. P.; Stevens, J. S.; Towler, M.; Wood, P. A.; *J. Appl. Crystallogr.* **2020**, *53*, 226. [Crossref]
73. Ellman, G. L.; Courtney, K. D.; Andres, V.; Featherstone, R. M.; *Biochem. Pharmacol.* **1961**, *7*, 88. [Crossref]
74. Simas, A. M.; Rocha, G. B.; *Semi-Empirical Methods for Electronic Structure in Quantum Chemistry*; Livraria da Física Publisher: São Paulo, 2007.
75. Guex, N.; Peitsch, M. C.; *Electrophoresis* **1997**, *18*, 2714. [Crossref]

Submitted: February 12, 2026
Final version online: April 10, 2026